Magma crystallization and viscosity: A study of molten basalts from the Piton de la Fournaise volcano (La Réunion island)

Nicolas Villeneuve, Daniel-R. Neuville, Pierre Boivin, Patrick Bachèlery, Pascal Richet

Magma crystallization and viscosity: A study of molten basalts from the Piton de la Fournaise volcano (La Réunion island)

Nicolas Villeneuve[a], Daniel R. Neuville[b], Pierre Boivin[c], Patrick Bachèlery[d], Pascal Richet[b]

[a]Centre de Recherche en Géographie de l'Université de La Réunion, 15 avenue René Cassin, 97715 Saint-Denis Msg 9, La Réunion, France
[b]Physique des Minéraux et des Magmas, Institut de Physique du Globe de Paris, 4 place Jussieu, 75252 Paris Cedex 05, France
[c]Laboratoire Magmas et Volcans, Université Blaise Pascal 5 rue Kessler, 63038 Clermont-Ferrand, France
[d]Laboratoire GéosSciences Réunion, Institut de Physique du Globe de Paris, Université de La Réunion, CNRS, URM 7154-Géologie des Systèmes Volcaniques, 15 avenue René Cassin, 97715 Saint-Denis Msg 9, La Réunion, France

The viscosity of three molten basalts produced by fusion of lavas issued from different eruptions of the Piton de la Fournaise (La Réunion island) has been investigated above the liquidus and at high degrees of supercooling. For all basalts, crystallization took place rapidly above the glass transition range, which made static measurements problematic because of time-dependent, non-Newtonian rheology. By contrast, reproducible results were obtained in dynamic measurements made at a constant heating rate of 5 K/mn. Partial crystallization resulted in strong viscosity increases which were primarily due to the presence of solid inclusions. Comparisons with phase equilibria experiments performed for the same samples at higher temperatures show that crystallization takes place differently below the liquidus and at strong degrees of supercooling. As recently described for simpler systems, these differences in nucleation and growth are controlled by the relative mobilities of the cations diffusing within the melt to attach themselves to crystal–melt interfaces. A consequence is that the composition evolution of the residual melt differs in equilibrium and irreversible crystallization. In turn, this contrast induces opposite viscosity variations for the residual melt.

1. Introduction

Whether at mid-ocean ridges, in traps, or in shield volcanoes, basalt is clearly the most important lava type on Earth. Because viscosity is the single most important property controlling magma transport at all scales from the source to the surface, numerous measurements have been performed on molten basalts either in the field (e.g., Gauthier, 1973; Pinkerton and Norton, 1995) or in the laboratory (e.g., Shaw, 1969; Murase and McBirney, 1973; Giordano and Dingwell, 2003). General agreement is not found between these results, however, because of differences in overall chemical composition, or because variable fractions of gaseous bubbles and solid inclusions can also strongly affect viscosity (e.g., Ryerson et al., 1988; Lejeune and Richet, 1995; Lejeune et al., 1999; Saar et al., 2001; Sato, 2005; Ishibashi and Sato, 2007).

To understand better the complex interplay of viscosity and crystallization, we have studied a series of lavas from the Piton de la Fournaise, one of the most active volcanoes on Earth for which measurements were lacking. Although lavas issued during a given eruption present the great chemical and petrological homogeneity of the so-called steady state basalts (Albarède et al., 1997), their composition, crystal fraction and macrocryst content may vary markedly from an eruption to another. In addition to their direct volcanological bearing (Villeneuve, 2000), viscometry experiments on these lavas can thus have a broader interest in view of the wide range of conditions that can be investigated. As an example, the effects of variable MgO contents can be studied simply up to values higher than typically found in basalts.

To cope with the recent diversity of Piton de la Fournaise lava compositions (Table 1), we selected four different basalts which sampled the 1977–1998 activity cycle of the volcano (Boivin and Bachèlery, submitted for publication): (i) an olivine basalt from the 1986 flow in Takamaka Ravine (Ba86); (ii) an aphyric basalt from the 1983 lava flow on the Southern part of the Dolomieu Crater (Ba83); (iii) an almost aphyric basalt from the 1998 lava flow of the Piton Kapor, on the Northern part of the Dolomieu Crater (Ba98); (iv) and, for comparison, a picritic basalt (oceanite) from the 1977 flow of Piton Sainte-Rose (O77) as an extreme case of MgO enrichment. Although the compositions of Ba83 and Ba98 are very similar, both were investigated because the latter differ from the former by its unusually high plagioclase content (Boivin and Bachèlery, submitted for publication).

* Corresponding author. Present address: Institut de Recherche pour le Développement, US 140 ESPACE, BP172, 97492 Sainte-Clotilde cedex, France.
E-mail address: nicolas.villeneuve@univ-reunion.fr (N. Villeneuve).

Table 1
Chemical composition and phase proportions[a] of basalt samples (wt.%)

	O77	Ba86	Ba83	Ba98[b]	SGBa98	SFB[c]
SiO_2	44.60	47.78	48.74	48.74	57.36	46.58
Al_2O_3	9.03	13.68	14.89	14.53	12.18	13.28
Fe_2O_3 total	14.22	12.80	12.21	12.61	12.45	9.30
MgO	21.14	9.13	6.42	6.52	3.52	9.15
CaO	7.36	10.93	11.62	11.03	7.88	10.00
Na_2O	1.57	2.47	2.68	2.61	4.13	5.60
K_2O	0.47	0.74	0.80	0.67	1.74	1.38
TiO_2	1.67	2.56	2.74	2.58	2.80	2.45
P_2O_5	0.37	0.48	0.46	0.45	1.27	
MnO	0.18	0.17	0.16	0.16	0.43	
LoI[d]	0.00	0.00	0.00	0.00	0.08	
Total	99.94	99.93	99.96	99.95	99.90	99.64
ρ (g/cm^3)[e]	3.04	2.83	2.82	2.81	2.57	2.86
Glass	41	88	79	82		
Olivine	45	2	8	4		
Pyroxene	6	9	5	4		
Plagioclase	7	1	7	10		
Spinel	2	0	2	1		

[a] For samples collected in the field (Albarède and Tamagnan, 1988).
[b] Sample quenched from around 1420 K.
[c] Stein Frentz alkali basalt from Bouhifd et al. (2004).
[d] Loss on ignition.
[e] Room-temperature Archimedean density of glass samples.

As a matter of fact, partial crystallization of these melts is ready in the supercooled liquid state and exerts a strong effect on viscosity. As observed for simpler melts (Roskosz et al., 2005, 2006), however, the crystals that precipitate at strong degrees of supercooling and near the liquidus differ markedly. We have thus documented these differences for the same series of samples by combining phase equilibria determinations near the liquidus with characterization of the crystals that formed near the glass transition. Comparisons between the results of these two kinds of experiments thus give a more complete picture of the possible influence of partial crystallization on the viscosity of basalt melts. Actually, near the glass transition this influence is similar to that previously observed for an alkali basalt (Bouhifd et al., 2004) in spite of differences in mineral compositions. This similarity suggests that, other things being equal, the manner in which composition affects viscosity, either directly or through partial crystallization, is weak, not only for Piton de la Fournaise magmas but also for other kinds of basalt melts. In view of the irreversibility of crystallization, however, predicting the nature and composition of the phases that form, and their effect on non-Newtonian viscosity at large crystal fractions, remains intrinsically difficult.

2. Experimental methods

2.1. Samples and characterization

The chemical compositions of the samples investigated are listed in Table 1 together with their crystal fractions as determined by optical counting. The olivine macrocrysts, which are especially abundant in the Ba77 sample, grew in magma chamber and were flushed out along with the magma only when the flow rate were was high. Picritic slurries have thus been observed during some major magma surges (Albarède et al., 1997). Microcrystalline phases, i.e., plagioclases, clinopyroxenes (CPX), olivines and spinels, are included in the mesostasis. Most of the natural samples could not be investigated by viscometry because cylindrical samples cored from such materials generally underwent first irregular deformation and then failure when the stress applied was increased above about $4\ 10^7$ Pa.

Such problems were previously encountered for other natural samples such as Etna basalts and Montagne Pelée andesites (Lévesque, 1999). After grinding in an agate mortar, we thus melted the Ba83, Ba86 and Ba98 lavas in a platinum crucible at 1870 K for a few hours in air, i.e., about 400 K above the liquidus temperatures. To ensure homogeneity, these fluid melts were stirred a few times. After rapid cooling in graphite molds resting on a copper plate, the samples were annealed overnight at around 850 K to remove internal stresses. Cylindrical samples were cored in the thick glass lenses obtained. The homogeneous nature of the glasses was apparent in the X-ray powder diffraction patterns recorded for each sample where only a few reflections of the aluminum sample holder were detected (see below). To distinguish these remelted samples from the Ba83, Ba86 and Ba98 starting lavas, we denoted them as GBa83, GBa86 and GBa98, respectively.

To provide a more detailed picture of the physical and chemical effects on viscosity, we measured the viscosity of a synthetic sample whose composition mimics that of the residual melt of the Ba98 sample under equilibrium subliquidus conditions at 1373 K. This SGBa98 sample was synthesized from oxide and carbonate mixes as described in previous papers (e.g., Neuville and Richet, 1991). Its composition could not be determined from electron microprobe analyses of the Ba98 sample because the scale at which the natural glass was free from microlites was too small with respect to the size of the electron beam. We thus used the Melts software (Ghiorso and Sack, 1995) to estimate it for a basalt having the Ba98 overall composition. This composition, which is included in Table 1, refers to a 43/57 melt–crystal fraction.

For samples run in viscometry, the room-temperature density was measured with an Archimedean method, toluene being used as the immersion liquid (Richet et al., 2000). Powder X-ray diffraction patterns were recorded at the Laboratoire de Minéralogie of Université Paris VI, with a Cu source and Si as an internal standard. Assignment of reflections and determination of unit-cell parameters were made with the MacDiff software (R. Petschick, Frankfurt Universität) and, for part of the samples, confirmed by Rietveld analyses.

Finally, two samples were examined by transmission electron microscopy with a Philips CM30 apparatus operated at 300 kV at the Centre commun de microscopie électronique (CCME) of the University of Lille. Electron diffraction patterns were recorded for selected crystals. We also made quantitative chemical analyses with an energy dispersive spectroscopy attachment, in the scanning mode, and a Noran X-ray Si detector with an ultrathin window. We calculated atom fractions with the Vantage software (version 2.3.2) and determined K-factors from silicate standards by the parameterless method (Van Cappellen, 1990). These results were corrected for absorption, the sample thickness being determined from the principle of electroneutrality (Van Cappellen and Doukhan, 1994). To check the precision of the measurements, we analysed analyzed the overall composition of the samples over a spot size much larger than the size of the crystals. For the GBa86 sample, the oxide content for instance agreed to within 1 wt wt.% with the data of Table 1, except for the K_2O and MgO contents which were too high by 2 and 3 wt wt.%, respectively, because of volatilization under the highly accelerated electron beam.

2.2. Phase equilibria experiments

Phase relations were determined for the natural materials with the apparatus described by Soulard et al. (1992). This setup consists of a 5-cm wide alumina tube, heated by a vertical water-cooled furnace, through which a controlled gas mix flows. Four different samples were run at the same time. Temperatures were measured in between the samples with an alumina sheathed PtRh6%–PtRh30% thermocouple put at the center of the sample holder which was located at the middle of the alumina tube. A water bath placed under the furnace allowed the ~3-mm in diameter capsules to be rapidly quenched at the end of the experiments. The run duration was long enough for solid–melt equilibrium to be achieved (Soulard et al., 1992; Desgrolard, 1996). It

varied from 96 h at 1049 K to 27 h at 1374 K and 4 h at 1477 K. At the end of the experiments the samples had sintered to form small pellets.

The oxygen fugacity determines the iron redox state and consequently influences the nature and composition of the crystallizing phases. In our experiments, the oxygen fugacity was controlled by mixtures of CO_2 and H_2 which ensured redox conditions close to those of the Ni–NiO buffer which are the relevant ones to Piton de la Fournaise basalts (Boivin and Bachèlery, submitted for publication). The appropriate gas fluxes were determined from the tables published by Deines et al. (1974). As a check, a test Ni–NiO buffer was inserted in the sample holder along with the investigated samples.

For the phase relation experiments, the lavas were simply ground to a grain size of less than 20 μm. Care being taken not to fractionate the different constituent minerals, the powders were shaped with polyvinyl alcohol as ~3 mm beads around a platinum wire. Experiments were made at room pressure under dry conditions because lavas erupting from the Piton de la Fournaise are essentially anhydrous. For lavas erupted over a period of 300 years, Semet (pers. comm.) has for instance derived mean values of 0.22 wt.% for H_2O^+ and of 0.07 wt wt.% for H_2O^- from analyses made on 84 and 47 samples, respectively.

The nature and composition of the crystalline phases were determined isothermally from about 1373 to 1523 K at 25 K intervals. After quenching in water, each sample was first observed by optical microscopy. Examination of crystalline phases did not show nonequilibrium phase relations as would have been indicated by the occurrence of an irregular morphology. The chemical composition of the various phases was then determined from electron microprobe analyses made with a CAMECA SX100 probe operated at 15 kV and 12 nA. About 10 different analyses were made for each pellet for Si, Al, Fe, Mg, Ca, Na, K, Ti, Mn and Cr. To determine the relative proportions of phases, we minimized mass balance equations of the form

$$C_i^n = \sum X_p C_i^p \quad (1)$$

where C_i^n and C_i^p are the weight fraction of oxide i in the material and in phase P, respectively, and X_p the weight fraction of phase P in the material.

2.3. Viscometry

Viscosity (η) was measured near the glass transition range and at superliquidus temperatures. From 10^9 up to 10^{14} Pa s, the measurements were made with the creep apparatus described by Neuville and Richet (1991) whereby the rate of deformation of a sample is determined as a function of the uniaxial stress (σ) exerted at a given temperature T. Cylindrical samples, 10-mm long and 5 mm in diameter, were investigated in air. The viscosity was given by:

$$\eta = \sigma l/3(\mathrm{d}l/\mathrm{d}t), \quad (2)$$

where t is time and l is the length of the sample.

Two kinds of measurements were made with this method. Isothermal, static experiments were performed at several constant stresses ranging from $5\,10^5$ (at the lowest viscosities) to $5\,10^7$ Pa (at the highest viscosities) to check the Newtonian nature of rheology. At a single stress of about 10^6 Pa, we also made dynamic measurements with a heating rate of 5 K per minute as described by Bouhifd et al. (2004). Experiments on the NBS 717 standard glass showed that the latter method gives results accurate to better than 0.04 log unit as found for static experiments (Neuville and Richet, 1991).

Finally, high-temperature viscosities were measured in air between 1400 and 1700 K to within 0.04 log unit with the concentric viscometer described by Sipp et al. (1997). The melt was contained in a 29-mm i.d. Pt–Ir10% crucible. The torque needed to rotate a 14-mm o.d. Pt–Rh20% spindle immersed in the liquid at given speed was measured with a Rheomat 115 viscometer head. Again, the Newtonian nature of viscosity was checked through measurements made at about 10 different speeds which ranged, depending on temperature, from 0.05 to 780 rpm. In view of the slight composition dependence of basalt viscosity above the liquidus, measurements were performed on the single GBa98 sample.

2.4. Iron redox state

The iron redox ratio of the viscometry samples was determined to within ±0.02 with the wet chemical method described by Wilson (1960). Although iron was primarity primarily reduced in the remelted basalts (Table 2), some differences in redox ratios resulted from differences in heating duration and crucible size. As previously reported by Bouhifd et al. (2004) for other basalt samples, no significant change in the iron redox ratios were observed under the conditions of the creep experiments (Table 2). This is consistent with the kinetics of iron redox reactions determined in similar temperature intervals (Magnien et al., 2004, 2008) which are very slow for such large samples. As for the influence of redox state on viscosity near T_g, it amounted to less than a factor of ten between other basalt samples with $Fe^{3+}/\sum Fe$ ratios of 0.17 and 0.84 (Bouhifd et al., 2004).

In high-temperature viscometry no attempt was made at performing the measurements at constant redox ratio. Although the $Fe^{3+}/\sum Fe$ ratio of GBa98 would decrease from about 0.76 at 1450 K to 0.52 at 1650 K under equilibrium with air (Kress and Carmichael, 1991), such variations would induce minor viscosity changes in this temperature interval (Vignesoult and Thelohan, 1993; see also Bouhifd et al., 2004).

The redox ratio of the phase equilibria samples could not be determined because of their small size and of the destructive nature of wet chemical analyses. According to the model of Kress and Carmichael (1991), they ranged from 0.37–0.41 at 1527 K to 0.60–0.64 at 1375 K for the oxygen fugacities of the Ni–NiO buffer. The redox state of these samples was thus similar to that of the low-viscosity specimen and joined with those of the high-viscosity samples (Table 2). Such difference did not result in serious inconsistency between low- and high-temperature crystallization experiments. Whereas the kinetics of crystal nucleation and growth is higher for oxidized than for reduced basalt melts at high degrees of supercooling, the nature of the phases that form is in effect similar in both cases (Bouhifd et al., 2004).

3. Results

3.1. Phase relations

The phase assemblages observed at the various temperatures investigated are summarized in Table 3 and Fig. 1. The variations of the crystal fraction with temperature are shown in Fig. 2. For the Ba98 sample, they are illustrated in Fig. 3 by the electron microprobe observations made after quenching from four different run temperatures. Although the experiments were not reversed, the constancy of the phase composition observed in electron microprobe analyses and the "normal" partition coefficients found for Mg and Fe between olivine and the glass phase did not point to nonequilibrium effects. This statement is confirmed by the good agreement (Fig. 2) between

Table 2
Iron redox ratios of GBa83, GBa86 and GBa98 measured before and after low-temperature viscosimetry

Sample	$Fe^{3+}/\sum Fe_{init}$	$Fe^{3+}/\sum Fe_{fin}$
GBa83	0.31	0.32
GBa86	0.41	0.43
GBa98	0.26	0.28

Table 3
Proportion (wt.%) of phases in samples quenched from the temperatures indicated in phase equilibria experiments

Samples \T (K)		1374	1399	1425	1437	1452	1476	1527
O77	Glass	14.4	18.1	34.0	35.5	59.6	61.8	~65
	Olivine	45.5	43.5	41.3	41.8	37.7	35.9	
	CPX	15.8	15.3	8.9	8.5			
	Plagioclase	23.0	20.8	13.6	12.3			
	Spinel	1.0	1.2	1.3	1.2	1.8	1.8	
Ba83	Glass	34.2	57.9	75.5	92.0	99.9	100	
	Olivine	5.1	4.3	2.0	0.2			
	CPX	23.0	12.2	7.2				
	Plagioclase	34.6	23.9	15.1	6.5			
	Spinel	2.7	1.2	1.1	2.1			
Ba86	Glass	33.4	47.2	62.5	79.6	92.3	96.8	100
	Olivine	12.8	11.7	10.3	6.6	5.7	2.9	
	CPX	21.5	16.4	10.2	4.7			
	Plagioclase	29.2	23.1	16.3	7.2			
	Spinel	2.4	1.1	0.7	2.9	1.6	1.3	
Ba98	Glass	42.2	55.8	76.8	90.1	94.0	100	
	Olivine	5.0	3.5	3.2	0.4			
	CPX	18.7	13.9	3.5	1.8			
	Plagioclase	32.3	25.0	14.9	6.1	3.8		
	Spinel	1.6	1.8	1.1	1.9	1.3		

the phase relations observed in our study and the predictions of the Melts model (Ghiorso and Sack, 1995).

The liquidus temperatures of the Ba86, Ba83 and Ba98 samples were about 1530, 1450 and 1480 K, respectively. At temperatures ranging from 1400 to 1450 K, these lavas were thus issued about 100 K at most below the liquidus. As a result of complete melting of the olivines and spinels present in the starting lavas, the composition of the glass phases is enriched in MgO, FeO and Cr_2O_3 compared to that of the matrix in the starting material. In contrast, the O77 sample did not melt completely even during experiments made at 1900 K. Such a very high liquidus temperature is of course spurious as it originates in the high olivine and spinel contents that results from addition of these macrocrysts to the original melt before the final ascent.

In the Ba98 sample, plagioclase is the first mineral to appear somewhat above 1448 K along with spinel. Olivine and clinopyroxene follow closely. Such early precipitation of plagioclase is also predicted by the Melts model (Ghiorso and Sack, 1995). Although it is not typical of recent Piton de la Fournaise lavas, this feature has been observed through optical microscopy on samples which, like Ba98, were issued after April 1998 when the chemical composition of the lava began to change significantly (Fig. 4). For instance, the MgO content increased from 6 to 7.5 wt.% whereas the SiO_2 content decreased correlatively from 49.5 to 48 wt wt.%. This evolution is likely due to mixing of a differentiated magma with a more primitive source during refeeding of the system (Vlastélic et al., 2005).

The crystallization pattern of Ba83 is more typical of steady state basalts. Spinel, the first mineral to precipitate, has been observed only below 1452 K. For Ba86, the first liquidus minerals are olivines and oxides which begin to form between 1527 and 1476 K. These high temperatures likely result from contamination of the melt phase by the olivine macrocrysts, albeit to a lesser extent than for O77 (Famin et al., submitted for publication). In all samples but Ba98, plagioclases appear between 1452 and 1438 K. For the O77 and Ba86 samples, they do so along with clinopyroxenes, whereas olivines and plagioclases precipitate in the same temperature interval in Ba83. In this sample, clinopyroxenes formed at lower temperatures that were close to 1425 K. For all samples, further experiments were performed at 1322 and 1348 K. The presence of a glass phase could no longer be observed by optical microscopy and no additional crystalline phases were detected. Below 1322 K, the crystal fraction was so high that electron microprobe analyses of the residual glass were impossible (Fig. 3d).

Overall, there is a definite similarity between the crystallization patterns of the four samples in that all crystals appear in a temperature interval of less than 100 K. Quantitatively, this similarity is borne out by the variations of the crystal fraction with temperature.

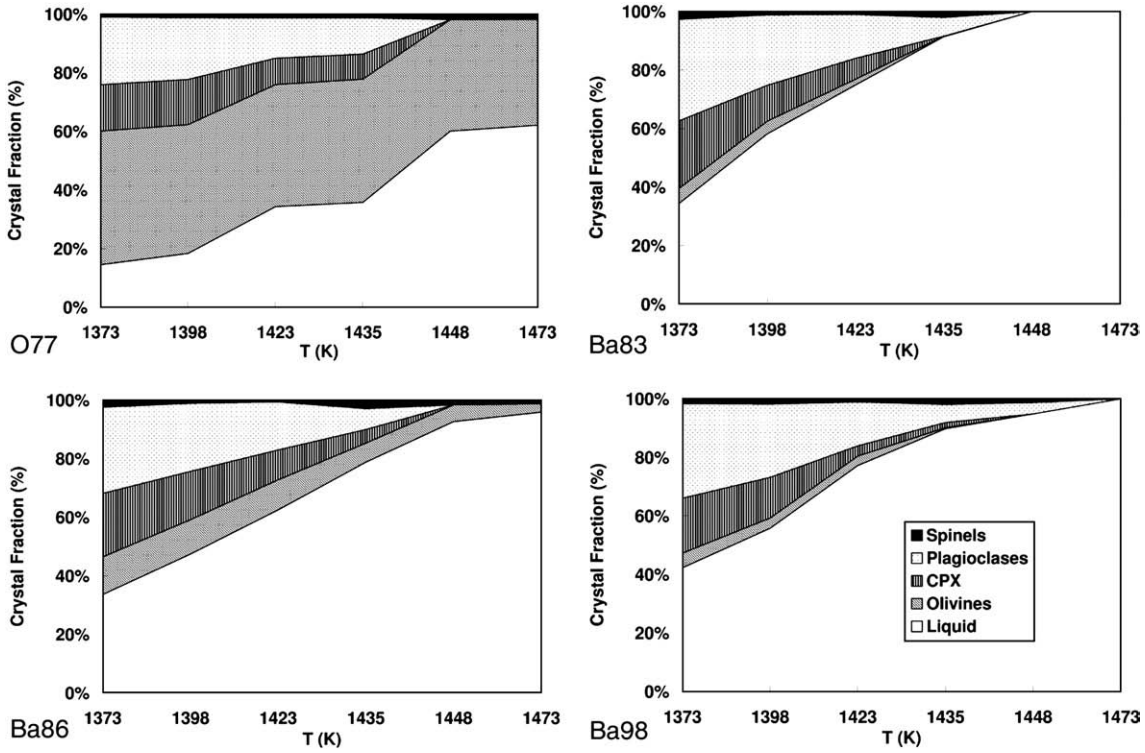

Fig. 1. Mineral proportions of the basalt samples at the temperatures investigated in phase equilibria experiments.

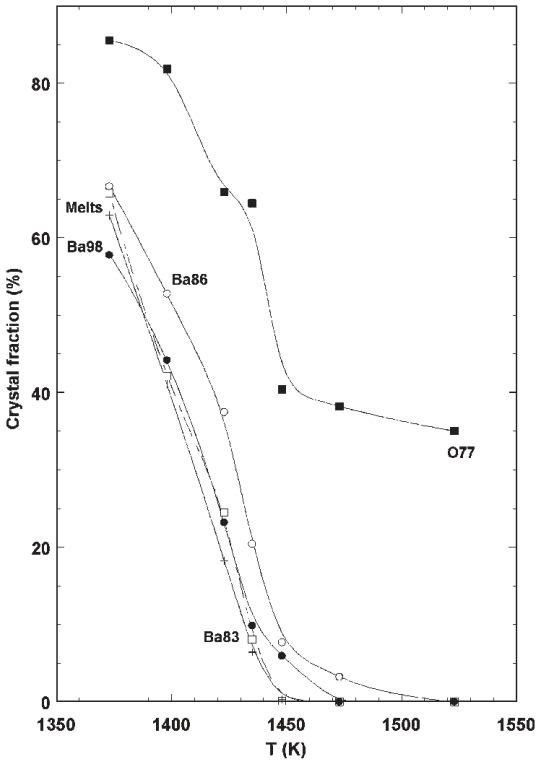

Fig. 2. Crystal fractions (wt.%) as a function of temperature for the compositions investigated. For comparison, the predictions of the Melts model (Ghiorso and Sack, 1995) are also plotted as a solid line for the Ba98 sample.

The crystal fraction first increases slowly with decreasing temperature down to about 1450 K, and then much more rapidly in an almost linear way. This change of course signals the beginning of cotectic crystallization when plagioclase and clinopyroxene precipitate along with olivine and spinel (Ludden, 1978). The trend shown by the O77 sample is similar to those observed for the other lavas except that, because of the abundance of olivine, the crystal fraction is much higher at a given temperature.

3.2. Viscosity

For natural samples, a few static viscosity experiments could be made only for Ba98 between 1020 and 1150 K in at constant stresses that ranged from 2.43 to 3.70 10^7 Pa. The viscosity was non-Newtonian because measurements could not be performed at lower stresses, but the range of conditions investigated was too narrow to determine stress–strain relationships. For the remelted basalts, Newtonian measurements could be made only for GBa98 sample. They are listed in Table 4 and plotted in Fig. 5 together with those made above the liquidus. The data cover a range of 12 orders of magnitude. To within their experimental uncertainties, they are reproduced by the empirical TVF equation

$$\log \eta = -4.52 + 5558/(T-582.9). \quad (3)$$

This equation yields 919 K for the standard glass transition temperature, at which the viscosity is 10^{12} Pa s. Static measurements were also made readily for the synthetic residual melt SGBa98. They are included in Table 4 and Fig. 5.

For the other remelted samples, static experiments were again beset by the extensive crystallization that took place over the few hours required to perform the measurements. That supercooling was extremely difficult above the glass transition was indicated by increases of viscosity with time of more than one order of magnitude at constant temperature which were similar to those described for molten andesite (Neuville et al., 1993) and basalt (Bouhifd et al., 2004). No limiting time-independent value was reached and, as previously

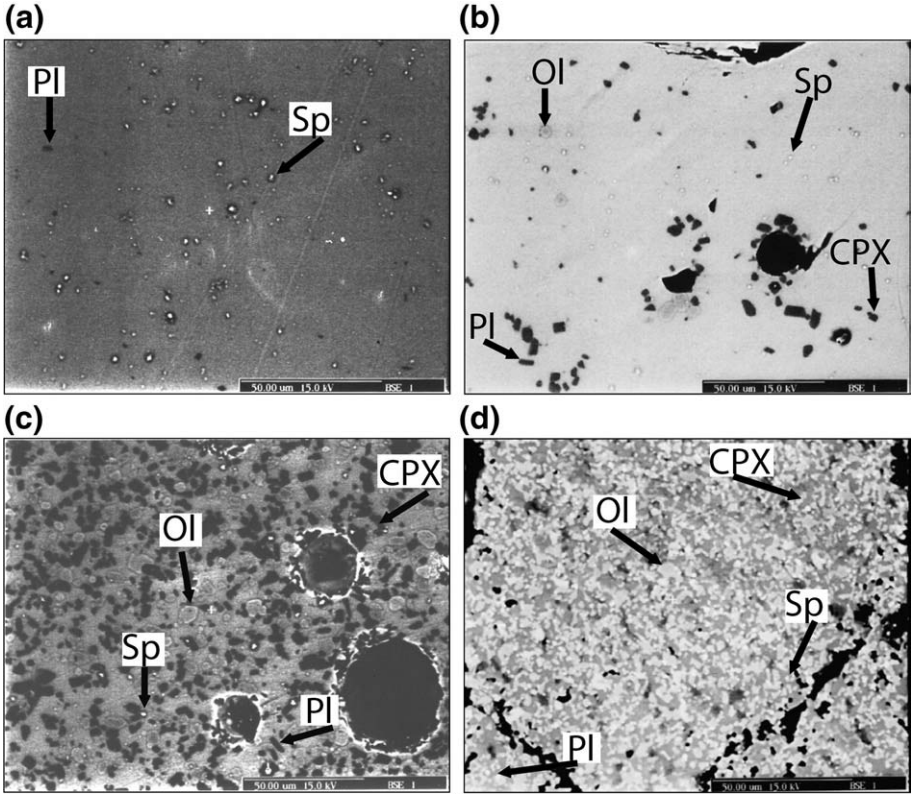

Fig. 3. Electron microprobe images of Ba98 samples after heating at 1452 K (a); 1437 K (b); 1399 K (c); and 1322 K (d). Symbols: Ol (olivines); Sp (spinels); Pl (plagioclases); CPX (clinopyroxenes).

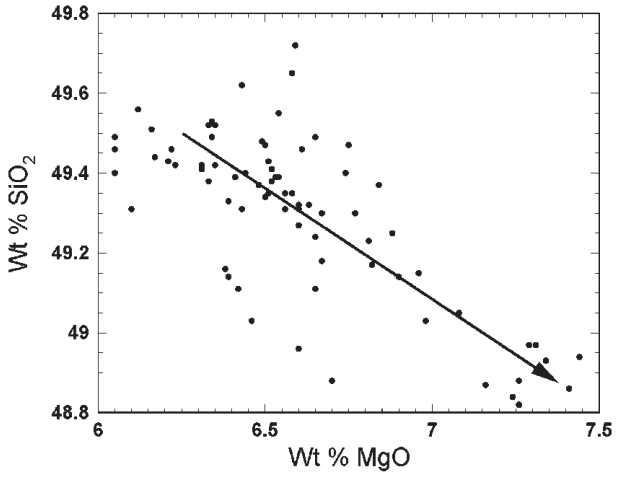

Fig. 4. Time evolution (arrow) of MgO and SiO_2 contents 178 days during the 1998 eruption of Piton de la Fournaise. Analyses from Semet et al. (see Villeneuve, 2000).

reported for crystal-bearing melts (Lejeune and Richet, 1995), the viscosity was markedly non-Newtonian. Nucleation and growth of crystals strongly depended on the temperature pathway followed during the measurements, which could not be controlled in the static mode. As a result, even the temperature dependence of viscosity at a given stress could not be determined in these experiments.

It is to obviate this problem that dynamic measurements were made on the GBa83, GBa86 and GBa98 samples. Since these experiments were made at constant stress, the departures from Newtonian viscosity could not be determined at higher crystal contents. From a practical standpoint, this was not a problem because of the intrinsic irreproducibility of such relationships when varying the experimental conditions. Consistent results were nonetheless obtained because the samples were large enough to ensure overall reproducible crystallization under strictly the same experimental conditions (Fig. 6). Although crystals could markedly differ by their chemical composition, their very small size did not prevent the products investigated from being homogeneous at the scale of the viscometry samples. Despite their compositional differences, the three samples yielded similar results which also agreed with experiments previously made on an alkali basalt sample (Bouhifd et al., 2004). As indicated by the good agreement found up to about 1080 K with the static results for GBa98 sample, Newtonian equilibrium viscosities were measured from 10^{12} to 10^{10} Pa s (Fig. 6a). On further heating, the

Table 4
Viscosity of the GBa98, SGBa98 and Ba98 samples (Pa s)

GBa98				SGBa98		Ba98	
T (K)	log η	T (K)	log η	T (K)	log η	T (K)	log η
919.8	12.04	954.3	10.36	1004.4	12.88		
922.3	11.87	956.9	10.27	1014.6	12.49	1051.4	13.34
924.8	11.68	959.5	10.23	1025.5	12.20	1077.4	13.07
927.5	11.61	962.1	10.13	1041.3	11.58	1108.7	12.21
930.0	11.49			1052.8	11.22	1108.7	12.43
932.5	11.36	1468.3	1.69	1057.6	11.06	1128.0	12.14
935.1	11.22	1492.7	1.69	1062.7	10.89	1128.0	11.92
937.9	11.13	1519.2	1.38	1068.0	10.72	1128.0	11.64
940.2	11.02	1546.3	1.24	1073.7	10.59	1148.6	11.59
941.4	11.00	1571.7	1.12	1078.4	10.47	1148.6	11.32
942.6	10.92	1593.1	1.00	1084.1	10.27		
944.0	10.91	1627.5	0.85	1094.3	9.95		
945.2	10.82	1639.0	0.78	1104.6	9.77		
946.6	10.68	1660.0	0.72	1114.4	9.43		
949.1	10.60			1125.4	9.17		
951.7	10.44			1135.8	8.97		

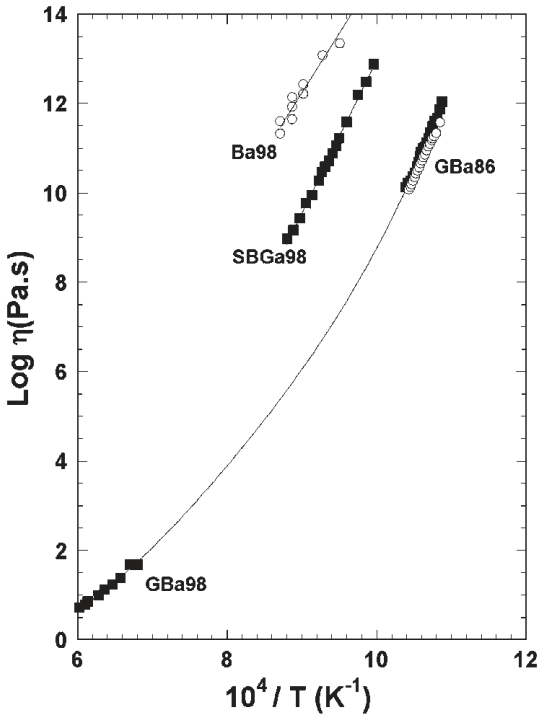

Fig. 5. Viscosity comparisons between basalt samples: GBa98 (remelted Ba98 lava), SGBa98 (residual melt of GBa98 after 57% crystallization at 1373 K), Ba98 (natural basalt with 18% crystallinity), GBa86 (remelted Ba86 lava). Open symbols: static measurements; solid symbols: dynamic measurements. The curve for GBa98 is the TVF equation fitted to the results.

viscosity increased markedly up to about $10^{11.5}$ Pa s before decreasing at temperatures higher than about 1150 K. These variations of course signal the occurrence of phase transformations which we investigated for the reference GBa98 sample.

For this purpose, we recorded the X-ray diffraction patterns of samples quenched at different key temperatures in duplicate experiments mimicking the viscometry time–temperature pathways. The sample A98 was the crystal-free starting material, whereas samples B98, C98 and D98 were taken at 1073 K, 1143 K and at the final temperature of 1273 K, respectively (Fig. 6a). The X-ray powder diffraction data indicate that spinel, with a unit-cell parameter a=8.3504 Å, was the first mineral to nucleate and grow near 975 K when the viscosity was about 10^{10} Pa s as indicated by the sharp departure from the data for the homogeneous melt (Figs. 6a and 7). Along with spinel, clinopyroxene then grew quickly from 1075 K, causing the sharp viscosity rise of two orders of magnitude up to 10^{11} Pa s observed near 1150 K (Fig. 6a). No additional phase formed at higher temperatures where the viscosity eventually decreased down to the value observed near 1075 K. From Rietveld analyses, we found that the clinopyroxene was fassaite, with lattice parameters a=9.7378, b=8.8628, c=5.3044 Å, and β=106.49°, and that spinel and fassaite were in a 1:8.3 volume ratio at the point D98 of Fig. 6a. The higher density of these crystals compared to the glass phase is reflected by the slight density increases apparent in Table 5.

For GBa86, the same conclusions were drawn from X-ray powder diffraction patterns recorded for samples quenched from the temperatures indicated in Fig. 6b and also from transmission electron microscopy observations. Given the overall similarity of the results, only the latter observations were made for GBa83. To maximize crystal size and, thus, to make chemical analyses possible, the samples investigated by TEM had been subjected to dynamic viscometry from 870 to 1300 K. The electron diffraction patterns recorded were characteristic of spinel and monoclinic pyroxene structures. Consistent with the X-ray results, most of the crystals investigated were

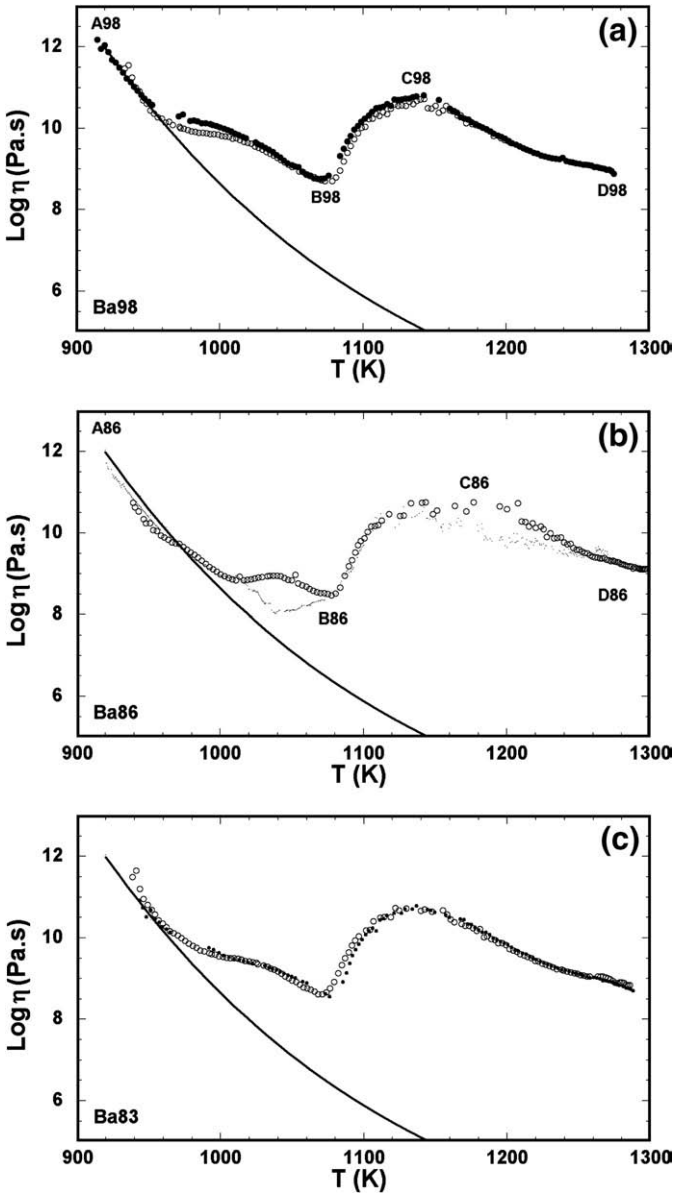

Fig. 6. Viscosity of samples measured dynamically. For comparison, the solid line represents the viscosity of the homogeneous melt GBa98 as given by the TVF Eq. (1). The labels indicate where samples were quenched for X-ray diffraction analysis in dummy experiments. (a) GBa98. (b) GBa86; (c) GBa83.

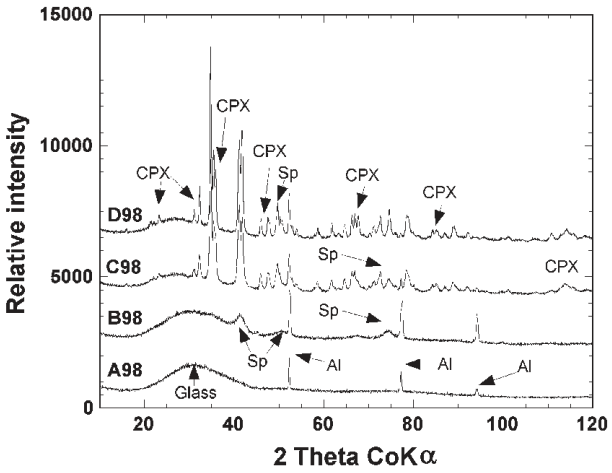

Fig. 7. Crystallization progress as seen in X-ray diffraction patterns recorded for GBa98 samples quenched from the different temperatures indicated in Fig. 6a. The Al peaks are those of the sample holder.

pyroxenes. In both GBa86 and GBa83 the crystal size was typically 50 nm, except for a few rod-shaped crystals whose length could reach 150 nm (Fig. 8). As a result, the chemical analyses were highly variable because glass was present in differing amounts in the analyzed spot.

For spinels, the composition could be determined from extrapolation down to 0 mol% SiO_2 of the mixing lines (originating from the overall sample composition) observed when the analyzed oxide mol fractions were plotted against silica content. For both Ba86 and Ba83 samples, the composition obtained was 55 mol% "FeO", 10 mol% Al_2O_3, 25 mol% MgO and 10 mol% TiO_2. Assuming arbitrarily that these spinels were a solution of spinel (s.s.), ulvöspinel, magnesioferrite and magnetite, we calculated a lattice parameter $a = 8.34$ Å from the data summarized by Deer et al. (1993), which agrees well with the observed value of 8.35 Å. Interestingly, a single spinel analysis yielded 1 mol% SiO_2, 65 mol% "FeO", 2 mol% Al_2O_3, 10 mol% MgO and 22 mol% TiO_2. Because the SiO_2 content, and thus glass contamination, was minimal, this result shows that spinels with differing compositions could form, reflecting the wide diversity of the composition fluctuations that can take place in the melt in the very first stage of spinel nucleation.

Unfortunately, the composition of pyroxenes could not be determined in a similar way from mixing lines because it did not differ considerably from that of the residual glass and also because the complex stoichiometry of such crystals prevented us from guessing the nominal content of any oxide. We could just conclude that these pyroxene compositions were more SiO_2-rich than observed by Bouhifd et al. (2004) for an alkali basalt. Likewise, analyses of the residual glass were highly variable because of the presence of crystals under the electron beam. As expected for irreversible crystallization, however, none of these analyses matched the composition of the equilibrium residual melt SGBa98.

Qualitatively, these observations conform to previous results according to which spinel is the first phase to nucleate and grow homogeneously in highly supercooled basalt melts (Beall and Rittler, 1976; Bouhifd et al., 2004). A pyroxene phase then forms heterogeneously at the contact of spinel crystals and grows rapidly in such a way that it constitutes most of the crystal fraction. A striking feature, however, is the fact that plagioclase scarcely precipitates in supercooled basalt melts even when after a high crystal fraction has been achieved through pyroxene formation (Fig. 3).

4. Discussion

4.1. Equilibrium vs. nonequilibrium crystallization

The fractions of glass and major minerals found in the starting lavas (Table 2) are only broadly consistent with our phase equilibria results

Table 5
Density of GBa98 and GBa86 at the temperatures shown in Fig. 6a and b

Sample	T	Density
A98	$<T_g$	2.814
B98	1073	2.824
C98	1143	2.944
D98	1273	2.953
A86	$<T_g$	2.827
B86	1049	2.828
C86	1073	2.872
D86	1143	2.994

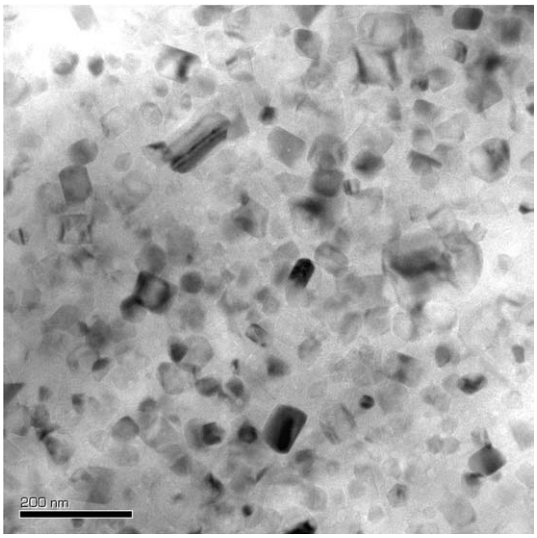

Fig. 8. Transmission electron microscopy observation of the GBa86 sample after dynamic viscometry up to 1300 K.

below 1430 K, a temperature which is typical of lavas erupting at the Piton de la Fournaise (Coppola et al., 2007). The consistency is best for O77 and Ba98, being somewhat coincidental in the former case. For both Ba83 and Ba86, the natural plagioclase contents are too low whereas either the olivine and or the CPX contents are content is too high for Ba83 and Ba86, respectively. These differences indicate that partial crystallization does not necessarily take place under near equilibrium conditions in the field. As to the lack of systematics embodied by the differences between Ba98, on the one hand, and Ba83 and Ba86, on the other, it suggests that the influence on partial crystallization of dissolved volatiles or differences in oxygen buffers, which were not investigated in our phase equilibria experiments, is not major.

There is in fact a striking contrast between equilibrium crystallization at high temperature and crystallization at high degrees of supercooling since only spinel and pyroxene crystallized during viscometry on GBa83, GBa86 and GBa98. By itself, this absence of plagioclase, which is the most abundant equilibrium phase (Fig. 1), demonstrates the irreversible nature of crystallization and indicates that the composition of the residual melt differs from that of the equilibrium liquid. This chemical effect has been investigated in detail by Bouhifd et al. (2004) for an alkali basalt melt. For samples quenched from 1100 K, transmission electron microscopy experiments showed that the volume fractions of the spinel and pyroxene phases were 1 and 40 vol.%, with crystal sizes of 35±15 nm and 10±5 nm, respectively. At 1300 K, the crystal sizes and volume fractions of spinel and pyroxene increased to 300 and 70 nm, and to about 5 and 55 vol.%, respectively. Our observed 1:8.3 volume ratio between spinel and pyroxene at 1273 K is consistent with these numbers.

According to recent work on simple aluminosilicate compositions (Roskosz et al., 2005), minerals precipitating at high degrees of supercooling are often metastable. They exhibit extensive nonstoichiometry and marked atomic disorder, contrasting with the stable and stoichiometric phases that crystallize near the liquidus. The observations made for basalt melts thus indicate that the same contrast is found in chemically complex systems. Its origin is the strongly temperature-dependent differences between the mobilities of network-forming and network network-modifying cations (Gruener et al., 2001). These differences are small near the liquidus where diffusion is fast for all cations so that crystals can grow to yield the stable phases. When the glass transition range is approached the mobility of cations decreases markedly (e.g., Mysen and Richet, 2005), but whereas the diffusivity of Ca^{2+}, Mg^{2+} and other network-modifying cations remain significant, that of the network-forming cations Si^{4+} and Al^{3+} become vanishingly low. Because the kinetics of crystal growth are limited by the rate at which atoms attach to the crystal–melt interface, the fastest diffusing elements find themselves enriched in crystals that turn out to be nonstoichiometric and disordered (Roskosz et al., 2005).

In other words, the phase transformations that take place in highly supercooled melts do not ensure minimization of the Gibbs free energy, but dissipates fastest the excess Gibbs free energy of the system. When pyroxenes are growing in supercooled basalt melts, the lack of plagioclase nucleation and growth, therefore, likely results from too slow diffusion of Si and Al. This feature is consistent with the calorimetric measurements performed by Lange et al. (1994) on an olivine basalt and on an ugandite which showed that clinopyroxene crystallization was the major factor determining the release of heat and, thus, causing a decrease enthalpy of the Gibbs free of the silicate system. Of particular interest is the fact that the extent of nonstoichiometry decreases regularly with increasing temperature until the liquidus is reached (Roskosz et al., 2006). In this respect, such a varying affinity of network network-modifying cations for the growing crystals might also affect trace elements whose partitioning between the molten and crystalline phases then could vary with temperature.

4.2. Rheology of homogeneous basalt melts

The basic problem raised by magma rheology is that measurements actually relevant to volcanology should refer to subliquidus conditions, where crystallization takes place, and not to superliquidus temperatures where they have generally been performed. Observations in the field are valuable because they are made under subliquidus conditions (e.g., Gauthier, 1973; Pinkerton and Norton, 1995), but they suffer from intrinsic difficulties compounded by a lack of experimental control. In fact, the narrow temperature intervals over which they are made and the differences in temperature, crystal content and other conditions make it difficult to use them for rationalizing rheology differences between different contexts.

Experimental control is of course tighter in laboratory measurements. In that case, however, a first difficulty is that the non-Arrhenian nature of viscosity makes it problematic to extrapolate to subliquidus conditions the quasi linear relationships between log viscosity and reciprocal temperature determined over restricted intervals above the liquidus. This is why measurements near the glass transition are of basic importance for ensuring reliable interpolations toward lower temperatures, through either empirical TVF equations (Fig. 5) or more fundamental expressions.

Measurements performed on a variety of basalts in fact point to a rather narrow viscosity domain for homogeneous melts (Fig. 9) if one discards earlier data that show an unusually high scatter or a clearly anomalous temperature dependence (e.g., Kani, 1934; Euler and Winkler, 1957). This is illustrated by data for molten basalts from Kilauea, Hawaii (Shaw, 1969), Columbia River and Galapagos (Murase and McBirney, 1973), Nova Bana, Czech Republic (Exnar and Voldan, 1982) and Etna (Lévesque, 1999; Giordano and Dingwell, 2003). As already noted, measurements made for various redox states of iron indicated a viscosity increase lower than one order of magnitude when the $Fe^{3+}/\sum Fe$ ratio of another molten basalt increased from 0.17 to 0.84 (Bouhifd et al., 2004), which is similar to the variations observed in simple systems (see review by Mysen and Richet, 2005). Hence, changes in the redox state or in the contents of MgO and other important oxides induce viscosity variations that are not large enough to warrant further discussion. We prefer to emphasize that the TVF Eq. (3) provides a general description of the viscosity of basalt melts and, in particular, that it represents a reliable starting point for evaluating the effects of solid inclusions due to partial crystallization.

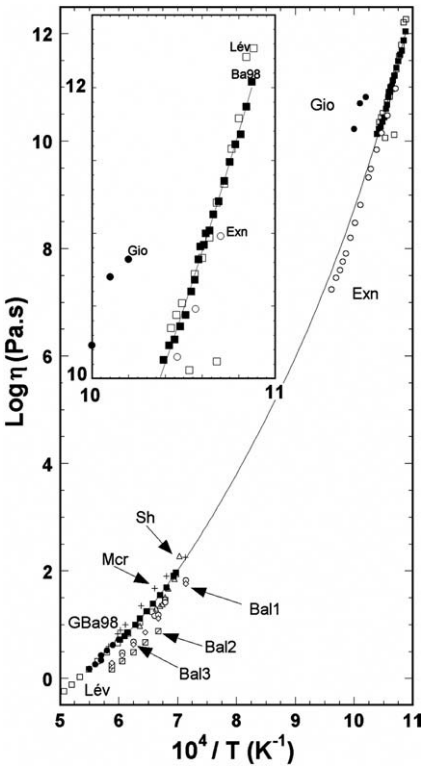

Fig. 9. Comparison between the viscosities of various basalt melts: GBa98 (experimental results and fitted TVF equation); Kilauea olivine tholeiite basalts: Shaw, 1969 (Sh); Etna basalts: Lévesque, 1999 (Lév) and Giordano and Dingwell, 2003 (Gio); Columbia River basalt: Murase and McBirney, 1973 (Mcr); alkali basalts: Exnar and Voldan, 1982 (Exn) and Bouhifd et al., 2004 (Bal), for samples with three different redox states.

4.3. Rheology of partially crystallized basalt melts

Partial crystallization of basalt melts affects viscosity in two ways, either through the physical effects due to the presence of solid inclusions or through the chemical effects caused by the composition changes of the residual molten phase. On both counts the chemical composition of basalt is a significant parameter as it determines the nature of the crystallizing phases and the composition variation of the residual melt. In general, however, investigation of crystallization effects on viscosity near the liquidus is made difficult by the difficulty of keeping the crystal fraction constant and the distribution of crystal and melts uniform (e.g., Ryerson et al., 1988). In some simple systems, the difficulty of separating the physical and chemical effects of crystallization can be obviated through experiments performed on congruently crystallizing compositions at high degrees of supercooling where crystal growth is negligibly low (Lejeune and Richet, 1995; Lévesque, 1999). Such measurements are fraught with difficulties for basalt melts, however, because crystallization takes place not only rapidly but also irreversibly in such a way that the residual liquid differs in composition from the equilibrium melt.

Experiments on simple melts indicate that physical effects are small at low enough crystal fraction, i.e., as long as the crystal percolation threshold is not reached (Lejeune and Richet, 1995). Under these conditions, the viscosity of partially crystallized melts remains close to Newtonian. Then, at constant chemical composition, physical effects can be accounted for with the so-called Einstein-Roscoe equation (Roscoe, 1952):

$$\eta = \eta_0 (1 - \phi/\phi_m)^{-n} \quad (4)$$

where η_0 is the viscosity of the homogeneous liquid, ϕ the volume crystal fraction and ϕ_m a critical crystal fraction above which flow would be impossible. There is an obvious trade-off between the exponent n of Eq. (4) and the ϕ_m parameter. Although the latter should depend on the shape and size distribution of crystals, values of 2.5 and 0.6, respectively, have been proposed for these parameters in silicate melts (e.g., Marsh, 1981; Lejeune and Richet, 1995). Before ϕ_m is approached, however, viscosity becomes so markedly non-Newtonian at crystal fractions higher than 30–40 vol.% that its prediction turns out to be difficult given the diversity of stress conditions that can prevail either in the laboratory or in the field (Ryerson et al., 1988; Lejeune and Richet, 1995; Lévesque, 1999).

More complex laws have nonetheless been proposed to account for the non-Newtonian nature of partially crystallized melts (Costa, 2005; Caricchi et al., 2007). But the general validity of such expressions or of universal stress–strain rate equations is doubtful, however, as indicated by experiments on partially molten $CaAl_2Si_2O_8$ (Lévesque, 1999) and on slightly supercooled basalt melts which showed a strong of the shape and size distribution of crystals (Sato, 2005; Ishibashi and Sato, 2007), two factors that may vary strongly from one system to another. The results obtained in this study at high degrees of supercooling might seem to be specially pertinent to vitroceramization processes, but the irreversible features seen in the phase proportions of the Ba83 and Ba86 basalts indicate that they are also relevant to some extent to lava flow. They confirm observations made on simple (Lejeune and Richet, 1995) or complex systems (Lévesque, 1999; Bouhifd et al., 2004) that the composition of the residual melt and the texture of the partially crystallized sample vary in such a way that different results are obtained when experiments are not made under identical conditions. The reason is the fact that the nature, composition and structure of crystallizing phases sensitively depend on thermal treatment when crystallization takes place in a strongly irreversible manner (e.g., Roskosz et al., 2005, 2006). The near impossibility of making reliable measurements on the natural starting materials is in fact another striking illustration of this point.

Concerning chemical effects, a general feature of partial crystallization is enrichment of the residual melt in SiO_2. Again, however, the resulting influence on viscosity depends on the equilibrium or irreversible nature of crystallization. Near 1100 K, the viscosity of the equilibrium residual SGBa98 melt is more than 3 log units higher than that of the homogeneous molten basalt (Fig. 5). For irreversible crystallization, in contrast, the viscosity of the liquid matrix unlikely increased with increasing crystal content as suggested by the similar variations determined under the same conditions by Bouhifd et al. (2004) for an alkali basalt. In the latter work the composition of the residual glass matrix was measured at five different steps of crystallization and the viscosity of synthetic liquids of these compositions was then measured. Although the SiO_2 content increased up to 75 wt wt.%, a decrease in alumina content coupled to an important enrichment in alkali oxides actually caused the viscosity of the liquid phase to decrease. Viscosity increases of about 6 log units similar to those of Fig. 6 were nonetheless observed for the partially crystallized melt, indicating that this chemical effect was clearly offset by the larger physical effects due to the presence of solid inclusions.

Finally, the O77 sample was included in this study as representative of the phenocryst-rich *oceanites* of the Piton de la Fournaise. We refer to Ryerson et al. (1988) for a discussion of the minimum ascent rates required to bring such phenonoliths to the surface. Here, we just note that these large olivine macrocrysts, which are roughly spherical, are distributed within a molten matrix whose intrinsic viscosity may remain close to that of Newtonian homogeneous molten basalts. As noted by Marsh (1981), for fractions approaching 60 vol.% the crystal contents would reach the critical fraction at which a disordered arrangement of spheres of equal sizes would prevent any flow. But the existence of a serial size distribution for these inclusions would make flow possible by increasing the effective critical fraction to values somewhat higher than 60 vol.%.

Acknowledgments

This paper is dedicated to the late J.-L. Cheminée who kept a constant interest in the senior author's thesis work. We thank Th. Staudacher for donating the Ba98 sample; D. Andrault for help with X-ray diffraction analyses; A. Addad and H. Leroux (CCME, University of Lille) for valuable help with the TEM experiments; A.-M. Lejeune, M. Roskosz and Th. Staudacher for stimulating discussions; and anonymous reviewers for thoughtful comments.

References

Albarède, F., Tamagnan, V., 1988. Modelling the recent geochemical evolution of the Piton de la Fournaise volcano, Réunion Island, 1931–1986. Journal of Petrology 29, 997–1030.

Albarède, F., Luais, B., Fitton, G., Semet, M., Kaminski, E., Upton, B.G.J., Bachèlery, P., Cheminée, J.-L., 1997. The geochemical regimes of Piton de la Fournaise Volcano (Réunion) during the last 530 000 years. Journal of Petrology 38, 171–201.

Beall, G.H., Rittler, H.L., 1976. Basalt glass ceramics. American Ceramic Society Bulletin 55, 579–582.

Boivin, P., Bachèlery, P., submitted for publication. Petrology of 1977–1998 Eruptions of Piton de la Fournaise, Réunion Island. Journal of Volcanology and Geothermal Research.

Bouhifd, M.A., Richet, P., Besson, P., Roskosz, M., Ingrin, J., 2004. Redox state, microstructure and viscosity of a partially crystallized basalt melt. Earth and Planetary Science Letters 218, 31–44.

Caricchi, L., Burlini, L., Ulmer, P., Gerya, T., Vassalli, M., Papale, P., 2007. Non-Newtonian rheology of crystal-bearing magmas and implications for magma ascent dynamics. Earth and Planetary Science Letters 264, 402–419.

Coppola, D., Staudacher, T., Cigolini, C., 2007. Field thermal monitoring during the August 2003 eruption at the Piton de la Fournaise (La Réunion). Journal of Geophysical Research 112, B05215. doi:10.1029/2006JB004659.

Costa, A., 2005. Viscosity of high crystal content melts: dependence on solid fraction. Geophysical Research Letters 32, L22308. doi:10.1029/2005GL024303.

Deer, W.A., Howie, R.A., Zussman, J., 1993. An Introduction to the Rock-Forming Minerals, 2nd ed. Longman, Burnt Mill.

Deines, P., Nafziger, R.H., Ullmer, G.C., Woermann, E., 1974. Temperature–oxygen fugacity tables for selected gas mixtures in the system C–H–O at one atmosphere total pressure. Bulletin of the Earth and Mineral Sciences Experiment Station 88 129 pp.

Desgrolard, F., 1996. Pétrologie des laves d'un volcan intraplaque océanique: le Karthala. Ile de la Grande-Comore (R.F.I. des Comores). Thesis, Université Blaise Pascal, Clermont Ferrand, 177 pp.

Euler, R., Winkler, H.G.F., 1957. Über die Viskositäten von Gesteins und Silikatschmelzen. Glastechnische Berichte 30, 325–332.

Exnar, P., Voldan, J., 1982. Measuring viscosity with the penetration viscometer. Silikaty 26, 251–259.

Famin, V., Welsch, B., Okumura, S., Bachèlery, P., Nakashima, S., submitted for publication. Three differentiations of a single magma at Piton de la Fournaise volcano (Réunion hotspot). Geochemistry Geophysics Geosystems.

Gauthier, F., 1973. Field and laboratory studies of the rheology of Mount Etna lava. Philosophical Transactions of the Royal Society of London 274, 83–98.

Ghiorso, M.S., Sack, R.O., 1995. Chemical mass transfer in magmatic processes IV. A revised and internally consistent thermodynamic model for the interpolation and extrapolation of liquid–solid equilibria in magmatic systems at elevated temperatures and pressures. Contributions to Mineralogy and Petrology 119, 197–212.

Giordano, D., Dingwell, D.B., 2003. Viscosity of hydrous Etna basalt: implications for Plinian-style basaltic eruptions. Bulletin of Volcanology 65, 8–14.

Gruener, G., Odier, P., De Sousa Meneses, D., Florian, P., Richet, P., 2001. Bulk and local dynamics in glass-forming liquids: a viscosity, electrical conductivity, and NMR study of aluminosilicate melts. Physical Review B64 024206/1-5.

Ishibashi, H., Sato, H., 2007. Viscosity measurements of subliquidus magmas: alkali olivine basalt from the Higashi-Matsuura district, Southwest Japan. Journal of Volcanology and Geothermal Research 160 (3–4), 223–238.

Kani, K., 1934. The measurements of the viscosity of basalt glass at high temperature, I and II. Proceeding of the Imperial Academy of Tokyo 10, 29–32 and 79–82.

Kress, V.C., Carmichael, I.S.E., 1991. The compressibility of silicate liquids containing Fe_2O_3 and the effect of composition, temperature, oxygen fugacity and pressure on their redox states. Contributions to Mineralogy and Petrology 108, 82–92.

Lange, R.A., Cashman, K.V., Navrotsky, A., 1994. Direct measurements of latent heat during crystallization and melting of a ugandite and an olivine basalt. Contributions to Mineralogy and Petrology 118, 169–181.

Lejeune, A.-M., Richet, P., 1995. Rheology of crystal-bearing silicate melts: an experimental study at high viscosities. Journal of Geophysical Research 100, 4215–4229.

Lejeune, A.-M., Bottinga, Y., Trull, T., Richet, P., 1999. Rheology of bubble-bearing magmas. Earth and Planetary Science Letters 166, 71–84.

Lévesque, S., 1999. Rhéologie de silicates fondus et de laves partiellement cristallisées. Thesis, Université de Marne-la-Vallée. 157 pp.

Ludden, J.N., 1978. Magmatic evolution of basaltic shield volcanoes of Reunion Island. Journal of Volcanology and Geothermal Research 4, 171–198.

Magnien, V., Neuville, D.R., Cormier, L., Mysen, B.O., Briois, V., Belin, V., Pinet, O., Richet, P., 2004. Kinetics of iron oxidation in silicate melts: a preliminary XANES study. Chemical Geology 213, 253–263.

Magnien, V., Neuville, D.R., Cormier, L., Roux, J., Hazemann, J.-L., de Ligny, D., Pascarelli, S., Vickridge, I., Pinet, O., Richet, P., 2008. Kinetics and mechanisms of iron redox reactions in silicate melts: the effects of temperature and alkali cations. Geochimica et Cosmochimica Acta 72, 2157–2168.

Marsh, B.D., 1981. On the crystallinity, probability of occurrence, and rheology of lava and magma. Contributions to Mineralogy and Petrology 78, 85–98.

Murase, T., McBirney, A.R., 1973. Properties of some common igneous rocks and their melts at high temperatures. Geological Society of America Bulletin 84, 3563–3592.

Mysen, B.O., Richet, P., 2005. Silicate Glasses and Melts: Properties and Structure. Elsevier, Amsterdam.

Neuville, D.R., Richet, P., 1991. Viscosity and mixing in molten (Ca, Mg) pyroxenes and garnets. Geochimica et Cosmochimica Acta 55, 1011–1019.

Neuville, D.R., Courtial, P., Dingwell, D., Richet, P., 1993. Thermodynamic and rheological properties of rhyolite and andesite melts. Contributions to Mineralogy and Petrology 113, 572–581.

Pinkerton, H., Norton, G., 1995. Rheological properties of basaltic lavas at sub-liquidus temperatures: laboratory and field measurements on lavas from Mount Etna. Journal of Volcanology and Geothermal Research 68, 307–323.

Richet, P., Whittington, A., Holtz, F., Behrens, H., Ohlhorst, S., Wilke, M., 2000. Water and the density of silicate glasses. Contributions to Mineralogy and Petrology 138, 337–347.

Roscoe, R., 1952. The viscosity of suspensions of rigid spheres. British Journal of Applied Physics 3, 267–269.

Roskosz, M., Toplis, M.J., Besson, P., Richet, P., 2005. Nucleation mechanisms: a crystal-chemical investigation of phases forming in highly supercooled aluminosilicate liquids. Journal of Non-Crystalline Solids 351, 1266–1282.

Roskosz, M., Toplis, M.J., Richet, P., 2006. Kinetic vs. thermodynamic control of nucleation and growth in molten silicates. Journal of Non-Crystalline Solids 352, 180–184.

Ryerson, F.J., Weed, H.C., Piwinskii, A.J., 1988. Rheology of sub-liquidus magma 1. Picritic composition. Journal of Geophysical Research 93, 3421–3436.

Saar, M.O., Manga, M., Cashman, K.V., Fremouw, S., 2001. Numerical models of the onset of yield strength in crystal–melt suspensions. Earth and Planetary Science Letters 187, 367–379.

Sato, H., 2005. Viscosity measurement of subliquidus magmas: 1707 basalt of Fuji volcano. Journal of Mineralogical and Petrological Sciences. 100, 133–142.

Shaw, H.R., 1969. Rheology of basalt in melting range. Journal of Petrology 10, 510–535.

Sipp, A., Neuville, D.R., Richet, P., 1997. Viscosity, configurational entropy and structural relaxation of borosilicate melts. Journal of Non-Crystalline Solids 211/3, 281–293.

Soulard, H., Provost, A., Boivin, P., 1992. $CaO–MgO–Al_2O_3–SiO_2$ (CMAS) at 1 bar from low to high Na_2O contents: topology of an analogue for alkaline basic rock. Chemical Geology 96, 459–477.

Van Cappellen, E., 1990. The parameterless correction method. Microscopy Microanalysis Microstructures 1, 1–22.

Van Cappellen, E., Doukhan, J.-C., 1994. Quantitative transmission X-ray microanalysis of ionic compounds. Ultramicroscopy 53, 343–349.

Vignesoult, S., Thelohan, S., 1993. Influence of iron content and redox level on physical properties of glasses. Fundamentals of Glass Science and Technology. ESG, Venice, pp. 643–646.

Villeneuve, N., 2000. Apports multi-sources à une meilleure compréhension de la mise en place des coulées de lave et des risques associés au Piton de la Fournaise: Géomorphologie quantitative en terrain volcanique. Thesis, Institut de Physique du Globe de Paris, 374 pp.

Vlastélic, I., Staudacher, T., Semet, M., 2005. Rapid change of lava composition from 1998 to 2002 at Piton de la Fournaise (Réunion) inferred from Pb isotopes and trace elements: evidence for variable crustal contamination. Journal of Petrology 46, 79–107.

Wilson, A.D., 1960. The micro-determination of ferrous iron in silicate minerals by a volumetric and colorimetric method. Analyst 85, 823–827.